Aptamer and Antisense-Mediated Two-Dimensional Isolation of Specific Cancer Cell Subpopulations

Mahmoud Labib,[†] Brenda Green,[‡] Reza M. Mohamadi,[†] Adam Mepham,[‡] Sharif U. Ahmed,[†] Laili Mahmoudian,[†] I-Hsin Chang,[†] Edward H. Sargent,[§] and Shana O. Kelley*,[†,‡,‖,#]

[†]Department of Pharmaceutical Sciences, University of Toronto, Toronto, Ontario M5S 3M2, Canada
[‡]Institute for Biomedical and Biomaterials Engineering, University of Toronto, Toronto, Ontario M5S 3G4, Canada
Departments of [§]Electrical & Computer Engineering, [‖]Biochemistry, and [#]Chemistry, University of Toronto, Toronto, Ontario M5S 1A8, Canada

S *Supporting Information*

ABSTRACT: Cancer cells, and in particular those found circulating in blood, can have widely varying phenotypes and molecular profiles despite a common origin. New methods are needed that can deconvolute the heterogeneity of cancer cells and sort small numbers of cells to aid in the characterization of cancer cell subpopulations. Here, we describe a new molecular approach to capturing cancer cells that isolates subpopulations using two-dimensional sorting. Using aptamer-mediated capture and antisense-triggered release, the new strategy sorts cells according to levels of two different markers and thereby separates them into their corresponding subpopulations. Using a phenotypic assay, we demonstrate that the subpopulations isolated have markedly different properties. This system provides an important new tool for identifying circulating tumor cell subtypes.

Circulating tumor cells (CTCs) are rare tumor cells shed from primary and metastatic tumor sites into the circulation as viable or apoptotic cells. Their presence in blood correlates with increased metastatic burden and reduced time to relapse. As a result, their isolation and analysis as liquid biopsies present a powerful means to monitor tumors noninvasively.[1]

A single tumor can contain subclones with numerous phenotypes; as a result, a given patient's CTCs can possess heterogeneous subpopulations with variations relevant to the development of metastatic disease.[2] Furthermore, CTCs exhibit phenotypes that evolve while they are bloodborne, a fact that may lead to additional complexity. Isolation of CTC subpopulations, particularly metastasis-initiating cells (MICs), remains challenging, and as a result, few methods exist for the isolation of low numbers of cells based on the presence of multiple markers. Fluorescence-activated cell sorting has been used to isolate CTC subpopulations and establish increased metastatic potential of specific cell types;[3] however, this method does not possess sufficient sensitivity to be used with the low numbers of CTCs typically found in patient samples. It is thus critically important to develop new, high-sensitivity approaches for CTC subpopulation isolation.

Several techniques have been used to isolate bulk CTCs, including gradient centrifugation, dielectrophoresis, size-based exclusion, mRNA tagging, and affinity-based enrichment.[4] While most affinity-based methods use antibodies against surface antigens for capture,[5−9] the use of aptamers may be advantageous for several reasons. The small size (2−3 nm in diameter) of aptamers compared to antibodies (12−15 nm in diameter) could allow for more accurate quantification of the cell surface markers and enhanced resolution in identifying distinct subpopulations.[10] In addition, cells captured using aptamers can be released gently using nucleases or the aptamer's complementary strand,[11,12] whereas antibody-based capture requires a harsh proteolytic digestion for release, which can damage the extracellular domains of membrane antigens and subsequently confound immunocytochemical analysis.[13] Indeed, several microfluidic devices have been developed for isolation of CTCs using aptamers specific to PTK7,[11,14−16] EGFR,[17,18] PSMA,[19] EpCAM,[20,21] and other cancer-specific markers,[22] indicating that these receptors are powerful targets for affinity-based capture.

Here we report an aptamer-mediated, two-dimensional (2D) approach that isolates cancer cell subpopulations using a fluidic chip. DNA aptamers specific to cell-surface markers are utilized for cell capture followed by cell release using corresponding antisense oligonucleotides to enable 2D sorting. We leverage a microfluidic strategy that captures cancer cells with very high levels of specificity and sensitivity and couple this approach with a molecular capture and release strategy (Figure 1A). When the capture-and-release strategy is repeated using two different aptamers, it allows 2D separation and the isolation of discrete subpopulations with differing surface expression profiles. We show that the subpopulations isolated also exhibit different phenotypes when analyzed using an invasion assay.

Our 2D sorting approach relies on fluidic capture of cells tagged using aptamers bound to magnetic nanoparticles. The fluidic chip used in this work for magnetic capture features zones containing X-shaped microfabricated structures that create localized pockets of low velocity favoring the accumulation of nanoparticle-tagged cells (Figure 1B).[23] The first zone has a high linear velocity that only retains cells with a high abundance of magnetic nanoparticles (i.e., a high EpCAM level). These cells are captured in this zone since the retaining magnetic force overcomes the drag force associated with the locally high flow
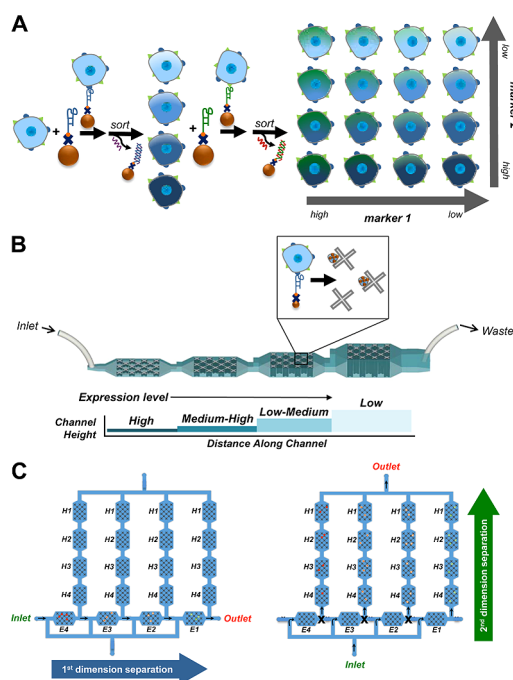
Figure 1. Schematic representation of the 2D sorting approach and chip. (A) Aptamer-mediated isolation of CTC subpopulations. Cells are first tagged with magnetic nanoparticles labeled with an aptamer specific to the first surface marker and sorted into four subpopulations using a fluidic device. The four subpopulations are then released using a complementary antisense DNA strand and subsequently tagged with magnetic nanoparticles labeled with an aptamer specific to the second surface marker. After sorting the captured cells into 16 subpopulations, cells are released using the complementary DNA strand to the second aptamer. (B) Design of four sequential zones that features four different average linear velocities (1×, 0.5×, 0.25×, and 0.125×) that facilitate the capture of differentially labeled cells. Cells with high expression levels of the surface marker are captured in the first zone, whereas cells with medium to low expression levels are trapped in later zones. (C) Schematic of the fluidic capture and subpopulation sorting strategy. Cells are first sorted according to EpCAM levels (E4 = high EpCAM, E1 = low EpCAM) and then HER2 levels (H4 = high HER2, H1 = low HER2). The workstation setup and open and closed configuration of valves are provided in Figures S1 and S2.

velocity. The ensuing three zones exhibit reduced linear velocities, each decreasing the velocity by a factor of 2. This design allows CTCs with high EpCAM levels and subsequently higher magnetic susceptibility to be trapped in the first zone, whereas cells with a lower expression level of EpCAM become trapped only in later zones based on the abundance of their surface EpCAM. After binning the subpopulations into four sequential zones, we release the cells using the antisense DNA strand complementary to the capturing aptamer. Cells released from the first, second, third, and fourth zone are denoted as E4, E3, E2, E1, respectively; where E denotes EpCAM and the number represents abundance (Figure 1C).

To facilitate separation in a second dimension, we tag the four subpopulations using magnetic nanoparticles labeled with aptamers specific for a different surface marker, e.g., HER2. Each subpopulation is binned in four sequential zones based on HER2 expression. Sixteen different subpopulations are then released from the respective zones using a DNA strand complementary to the HER2 specific aptamer. The discrete subpopulations obtained are labeled according to the expression

of the two markers; for instance, E1H1 denotes subpopulations showing a low expression level of both EpCAM and HER2.

The efficiency of cancer cell release and capture using the aptamer-mediated approach was investigated and optimized (Figure 2). Magnetic nanoparticles functionalized with strepta-
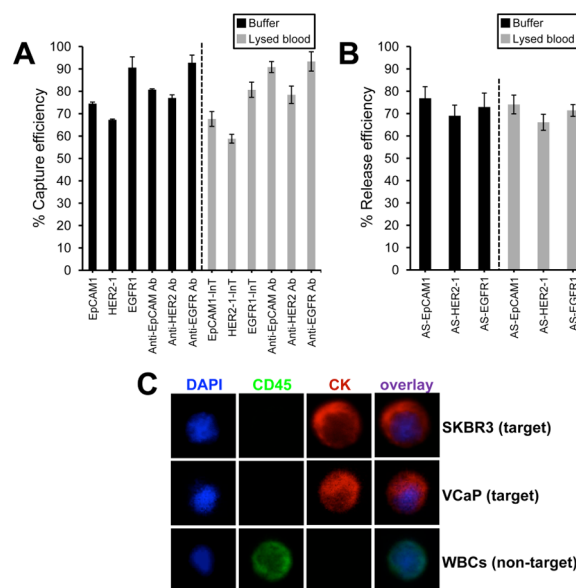

Figure 2. Performance of the aptamer-mediated capture and release approach in buffer and RBCs/WBCs-depleted blood. (A) Capture efficiency. The efficiency of capture mediated by aptamers bound to magnetic nanoparticles was compared to that observed with nanoparticle-bound antibodies. The device was loaded with either 1:1 mixture of target (SKBR3 or VCaP) cells and nontarget U937 cells (200 cells each) in buffer or 200 target cells spiked in blood. The EpCAM1 and HER2 aptamers and antibodies were tested using SKBR3 cells, whereas the EGFR1 aptamer and antibody were tested against VCaP cells. See Supporting Information for aptamer sequences. (B) Release efficiency. Release of captured cells was carried out using the corresponding antisense (AS) strand. The post-release cell count was calculated after cells were released, stained, and counted. All aptamers utilized in the blood experiments were modified with an inverted T at the 3′ terminus. (C) Cancer cell identification. An immunostaining approach was used to identify cancer cells. Only CK+/DAPI+/CD45− cells were counted when determining efficiencies.

vidin were conjugated to biotinylated aptamers, and overall capture in a 4-zone fluidic device was monitored. In these trials, SKBR3 cells (a breast cancer cell line) were used to assess capture efficiency mediated by the EPCAM and HER2 aptamers, and VCaP cells (a prostate cancer cell line) were used to test the EGFR aptamer. These cell lines were selected as they are known to express high levels of the surface markers of interest.[17−22] Levels of capture achieved with the aptamers were similar to what was observed with antibody-functionalized magnetic particles. Variations in sequence, linker chemistry, and length were tested to maximize capture efficiency (see Figures S3−S6). The maximum levels of capture that could be achieved were aptamer dependent, with the EGFR1 aptamer producing the highest levels of capture approaching 90%.

The optimization of antisense-triggered release (Figures 2B and S7−S9) included studies of antisense oligonucleotide concentration, incubation time, and flow rate, and release efficiencies approaching 80% were achieved under optimized conditions. The release of cells triggered by incubation with an exonuclease that would digest the aptamers was also tested.

Antisense-triggered release and exonuclease-mediated release achieved similar rates of release, and we thus conclude that the small number of cells that could not be liberated were irreversibly adsorbed to the chip surface.

An immunostaining approach was adopted to distinguish between cancer cells and white blood cells (WBCs), as shown in Figure 2C. Staining was performed with DAPI to identify nucleated cells, anti-CD45 to differentiate WBCs from cancer cells, and anticytokeratin (CK), as CK is a gold-standard marker for the identification of epithelial cells in the blood.[4] Only CK+/DAPI+/CD45− cells were counted as cancer cells.

We then proceeded to show that the performance was retained when the assay was carried out using blood samples. Because aptamers are rapidly degraded in whole blood even in the presence of nuclease inhibitors (Figure S10), it was necessary to employ modified aptamers to achieve satisfactory results with this sample type. Aptamers modified at the 3′ end with an inverted nucleotide (InT) performed well in lysed blood, as shown in Figures S11 and S12. These improved aptamers were tested for capture and release and yielded performance levels that approached what was attained with unmodified aptamers in buffered solution.

Proof-of-concept for aptamer/antisense-mediated sorting of 16 cancer cell subpopulations was obtained using two cell lines: SKBR3 and MDA-MB-361. SKBR3 cells have significantly higher levels of HER2 compared to MDA-MB-361, as shown using flow cytometry (Figure 3A,B). The 2D sorting profiles of the two cell
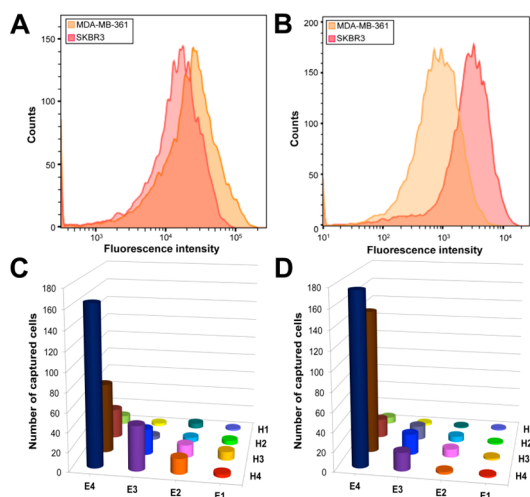

Figure 3. (A and B) Validation of the 2D sorting approach. Flow cytometric analysis of EpCAM (A) and HER2 (B) levels in SKBR3 and MDA-MB-361 cells. (C) Aptamer-mediated 2D isolation of 16 cell subpopulations from SKBR3 and (D) MDA-MB-361 cells. 1000 cells were tagged with magnetic nanoparticles and captured in the fluidic device. After releasing the cells using AS-EpCAM1, the cells were tagged with magnetic nanoparticles labeled with the HER2-1 aptamer and sorted. The 16 different subpopulations isolated were removed from the device for further characterization. See Figures S13 and S14 for data from C and D with error analysis.

lines, as shown in Figure 3C,D, reflect the lower HER2 expression on MDA-MB-361 cells and support the feasibility of using this approach to isolate subpopulations based on a dual-marker approach. 2D flow cytometric analysis of SKBR3 cells was also collected for comparison with the 2D sorting data, as shown in Figure S15. Additionally, profiling experiments of three breast cancer cell lines, including MCF7, SKBR3, and MDA-MB-231,

demonstrated that the cells are distributed in the microfluidic device based on their EpCAM expression level. The results corroborated the flow cytometry data (Figure S16).

The purity of captured cells from blood was also assessed. The 2D CTC sorting approach can deplete up to ∼99.99% of the WBCs (∼7,000,000 per mL of blood), after the first and second sorting steps (Figure S17). Also, the developed chip is capable of capturing a small number of VCaP cells (10 cells) from increasing volumes of blood (1−4 mL), as shown in Figure S18.

Flow cytometric analysis of EpCAM levels for the isolated subpopulations confirmed that the cells captured at the first zone exhibited the highest EpCAM level, whereas lower EpCAM expression was observed among cells collected from the following zones, as shown in Figure S20. The viability and proliferative capacity of the retrieved SKBR3 cell subpopulations were also determined after culturing the cells for 48 h in plates coated with collagen at 37 °C and 5% CO_2. The isolated subpopulations exhibited an average viability of 79 ± 1% and K_i-67 proliferative index of 42 ± 4%, as shown in Figures S21 and S22, respectively.

To assess whether the isolated subpopulations had detectable differences in phenotype, we characterized the ability of the cells to ingest fluorescent collagen. This assay is used to assess the invasiveness of cancer cells, since the ability to ingest collagen has previously been shown to correlate with the ability of cells to invade the extracellular matrix.[24] As shown in Figure 4A, flow
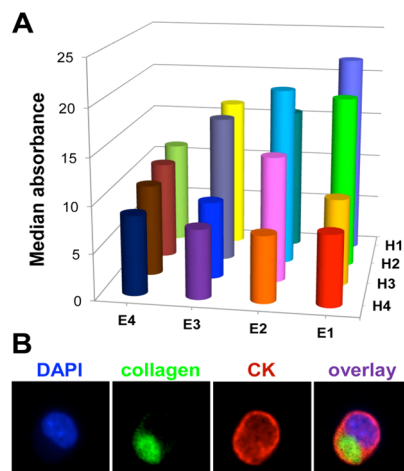

Figure 4. Isolated CTC subpopulations exhibit differing phenotypes. (A) Flow cytometric analysis of the collagen content of isolated cell subpopulations. Sixteen cell subpopulations isolated from the SKBR3 cell line were cultured on 12-well plates previously coated with 1 mL of 100 μg mL^{-1} FITC-collagen, in the presence of 1 mL of McCoy's medium modified containing 10% FBS and 1% penicillin-streptomycin for 48 h at 37 °C and 5% CO_2. Samples were analyzed with flow cytometry, and the absorbance values were normalized to the unstained control. See Figure S19 for data with error analysis. (B) Fluorescence microscope images for a DAPI+/collagen+/CK+ cell.

cytometric analysis of the collagen content for the subpopulations shows a marked difference in the behavior of different subpopulations. Cells that exhibited low EpCAM and HER2 levels exhibited much higher levels of collagen ingestion relative to cells with high or moderate levels. These results agree with previous studies showing that the expression of elevated levels of HER2 is usually associated with higher expression of the matrix metalloproteinases MMP2 and MMP9, which can accelerate the degradation of collagen.[25]

Finally, to demonstrate that the 2D sorting approach was effective in the analysis of samples collected from cancer patients, we analyzed the profiles of $CK^+/DAPI^+/CD45^-$ cells (i.e., putative CTCs) isolated from clinical samples. Samples were obtained from patients undergoing treatment for metastatic prostate cancer and subjected to 2D sorting using EpCAM and EGFR-targeted aptamers. As shown in Figures 5 and S23, we
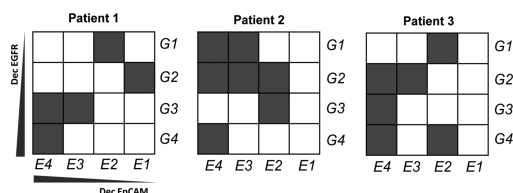

Figure 5. Isolated CTC subpopulations from clinical samples. Three blood samples collected from prostate cancer patients were sorted with anti-EpCAM and anti-EGFR aptamers and separated into 16 subpopulations. The shaded regions within the table indicate positive subpopulations. E denotes EpCAM and G denotes EGFR.

were able to isolate cell subpopulations exhibiting different expression levels of EpCAM and EGFR from the blood of each prostate cancer patient. While all of the patients were positive for high EpCAM, high EGFR cells (E4/G4), the other subpopulations present varied among the patients. This may reflect the heterogeneity of metastatic disease.

In conclusion, this new aptamer and antisense-mediated 2D subpopulation sorting technique can be used to isolate phenotypic subsets of CTCs defined by the expression level of two surface markers in a 2D format. The 2D capture and release enables isolation of CTCs with minimal contamination from the surrounding WBCs, thus paving the way toward molecular and functional analyses of CTCs.[26] While the isolation and clinical relevance of CTC subpopulations is a relatively new area, it is hoped that this method will allow an improved understanding of cancer progression, metastasis monitoring, and assessment of resistance to therapy in real-time to improve the clinical outcome. Further work will be required to establish the clinical relevance of the cells isolated using this method.

■ ASSOCIATED CONTENT

Ⓢ Supporting Information
Experimental details and data. The Supporting Information is available free of charge on the ACS Publications website at DOI: 10.1021/jacs.5b10939.

■ AUTHOR INFORMATION

Corresponding Author
*shana.kelley@utoronto.ca

Notes
The authors declare no competing financial interest.

■ ACKNOWLEDGMENTS

■ REFERENCES

(1) Alix-Panabieres, C.; Pantel, K. *Nat. Rev. Cancer* **2014**, *14*, 623.

(2) Yu, M.; Bardia, A.; Wittner, B. S.; Stott, S. L.; Smas, M. E.; Ting, D. T.; Isakoff, S. J.; Ciciliano, J. C.; Wells, M. N.; Shah, A. M.; Concannon, K. F.; Donaldson, M. C.; Sequist, L. V.; Brachtel, E.; Sgroi, D.; Baselga, J.; Ramaswamy, S.; Toner, M.; Haber, D. A.; Maheswaran, S. *Science* **2013**, *339*, 580.

(3) (a) Zhang, L.; et al. *Sci. Transl. Med.* **2013**, *5*, 180ra48. (b) Baccelli, I.; et al. *Nat. Biotechnol.* **2013**, *31*, 539.

(4) Green, B. J.; Saberi Safaei, T.; Mepham, A.; Labib, M.; Mohamadi, R. M.; Kelley, S. O. *Angew. Chem., Int. Ed.* **2016**, *55*, 1252.

(5) Nagrath, S.; Sequist, L. V.; Maheswaran, S.; Bell, D. W.; Irimia, D.; Ulkus, L.; Smith, M. R.; Kwak, E. L.; Digumarthy, S.; Muzikansky, A.; Ryan, P.; Balis, U. J.; Tompkins, R. G.; Haber, D. A.; Toner, M. *Nature* **2007**, *450*, 1235.

(6) Balasubramanian, S.; Kagan, D.; Hu, C. M.; Campuzano, S.; Lobo-Castanon, M. J.; Lim, N.; Kang, D. Y.; Zimmerman, M.; Zhang, L.; Wang, J. *Angew. Chem., Int. Ed.* **2011**, *50*, 4161.

(7) Adams, A. A.; Okagbare, P. I.; Feng, J.; Hupert, M. L.; Patterson, D.; Gottert, J.; McCarley, R. L.; Nikitopoulos, D.; Murphy, M. C.; Soper, S. A. *J. Am. Chem. Soc.* **2008**, *130*, 8633.

(8) Schiro, P. G.; Zhao, M.; Kuo, J. S.; Koehler, K. M.; Sabath, D. E.; Chiu, D. T. *Angew. Chem., Int. Ed.* **2012**, *51*, 4618.

(9) Yoon, H. J.; Kim, T. H.; Zhang, Z.; Azizi, E.; Pham, T. M.; Paoletti, C.; Lin, J.; Ramnath, N.; Wicha, M. S.; Hayes, D. F.; Simeone, D. M.; Nagrath, S. *Nat. Nanotechnol.* **2013**, *8*, 735.

(10) Wang, S.; Wang, H.; Jiao, J.; Chen, K. J.; Owens, G. E.; Kamei, K.; Sun, J.; Sherman, D. J.; Behrenbruch, C. P.; Wu, H.; Tseng, H. R. *Angew. Chem., Int. Ed.* **2009**, *48*, 8970.

(11) Zhao, W.; Cui, C. H.; Bose, S.; Guo, D.; Shen, C.; Wong, W. P.; Halvorsen, K.; Farokhzad, O. C.; Teo, G. S.; Phillips, J. A.; Dorfman, D. M.; Karnik, R.; Karp, J. M. *Proc. Natl. Acad. Sci. U. S. A.* **2012**, *109*, 19626.

(12) Ma, H.; Liu, J.; Ali, M. M.; Mahmood, M. A.; Labanieh, L.; Lu, M.; Iqbal, S. M.; Zhang, Q.; Zhao, W.; Wan, Y. *Chem. Soc. Rev.* **2015**, *44*, 1240.

(13) Dharmasiri, U.; Njoroge, S. K.; Witek, M. A.; Adebiyi, M. G.; Kamande, J. W.; Hupert, M. L.; Barany, F.; Soper, S. A. *Anal. Chem.* **2011**, *83*, 2301.

(14) Sheng, W.; Chen, T.; Tan, W.; Fan, Z. H. *ACS Nano* **2013**, *7*, 7067.

(15) Sheng, W.; Chen, T.; Kamath, R.; Xiong, X.; Tan, W.; Fan, Z. H. *Anal. Chem.* **2012**, *84*, 4199.

(16) Xu, Y.; Phillips, J. A.; Yan, J.; Li, Q.; Fan, Z. H.; Tan, W. *Anal. Chem.* **2009**, *81*, 7436.

(17) Wan, Y.; Tan, J.; Asghar, W.; Kim, Y. T.; Liu, Y.; Iqbal, S. M. *J. Phys. Chem. B* **2011**, *115*, 13891.

(18) Wan, Y.; Liu, Y.; Allen, P. B.; Asghar, W.; Mahmood, M. A.; Tan, J.; Duhon, H.; Kim, Y. T.; Ellington, A. D.; Iqbal, S. M. *Lab Chip* **2012**, *12*, 4693.

(19) Dharmasiri, U.; Balamurugan, S.; Adams, A. A.; Okagbare, P. I.; Obubuafo, A.; Soper, S. A. *Electrophoresis* **2009**, *30*, 3289.

(20) Jung, Y. K.; Woo, M. A.; Soh, H. T.; Park, H. G. *Chem. Commun.* **2014**, *50*, 12329.

(21) Song, Y.; Zhu, Z.; An, Y.; Zhang, W.; Zhang, H.; Liu, D.; Yu, C.; Duan, W.; Yang, C. J. *Anal. Chem.* **2013**, *85*, 4141.

(22) Shen, Q.; Xu, L.; Zhao, L.; Wu, D.; Fan, Y.; Zhou, Y.; Ouyang, W. H.; Xu, X.; Zhang, Z.; Song, M.; Lee, T.; Garcia, M. A.; Xiong, B.; Hou, S.; Tseng, H. R.; Fang, X. *Adv. Mater.* **2013**, *25*, 2368.

(23) (a) Mohamadi, R. M.; Besant, J. D.; Mepham, A.; Green, B.; Mahmoudian, L.; Gibbs, T.; Ivanov, I.; Malvea, A.; Stojcic, J.; Allan, A. L.; Lowes, L. E.; Nam, R. K.; Sargent, E. H.; Kelley, S. O. *Angew. Chem. Intl. Ed.* **2015**, *127*, 141. (b) Besant, J. D.; Mohamadi, R. M.; Aldridge, P.; Li, Y.; Sargent, E. H.; Kelley, S. O. *Nanoscale* **2015**, *7*, 6278.

(24) Friedlander, T. W.; Ngo, V. T.; Dong, H.; Premasekharan, G.; Weinberg, V.; Doty, S.; Zhao, Q.; Gilbert, E. G.; Ryan, C. J.; Chen, W. T.; Paris, P. L. *Int. J. Cancer* **2014**, *134*, 2284.

(25) Pellikainen, J. M.; Ropponen, K. M.; Kataja, V. V.; Kellokoski, J. K.; Eskelinen, M. J.; Kosma, V. M. *Clin. Cancer Res.* **2004**, *10*, 7621.

(26) Zhang, Y.; Zhou, L.; Qin, L. *J. Am. Chem. Soc.* **2014**, *136*, 15257.